# Assistance of Maltose Binding Protein to the in Vivo Folding of the Disulfide-Rich C-Terminal Fragment from *Plasmodium falciparum* Merozoite Surface Protein 1 Expressed in *Escherichia coli*†

Anne-Gaëlle Planson,*,‡ J. Iñaki Guijarro,§ Michel E. Goldberg,‡ and Alain F. Chaffotte‡

*Unité de Repliement et Modélisation des Protéines and Unité de Résonance Magnétique Nucléaire des Biomolécules, Dépt de Biochimie Structurale et Chimie, CNRS URA 2185, Institut Pasteur, 28 rue du Dr. Roux, 75015 Paris, France*

*Received July 24, 2003; Revised Manuscript Received September 15, 2003*

ABSTRACT: The C-terminal fragment of *Plasmodium falciparum* merozoite surface protein 1 (F19) is a leading candidate for the development of a malaria vaccine. Successful vaccination trials on primates, immunochemistry, and structural studies have shown the importance of its native conformation for its protective role against infection. F19 is a disulfide-rich protein, and the correct pairing of its 12 half-cystines is required for the native state of the protein. F19 has been produced in the *Escherichia coli* periplasm, which has an oxidative environment favorable for the formation of disulfide bonds. F19 was either expressed as a fusion with the maltose binding protein (MBP) or directly addressed to the periplasm by fusing it with the MBP signal peptide. Direct expression of F19 in the periplasm led to a misfolded protein with a heterogeneous distribution of disulfide bridges. On the contrary, when produced as a fusion protein with *E. coli* MBP, the F19 moiety was natively folded. Indeed, after proteolysis of the fusion protein, the resulting F19 possesses the structural characteristics and the immunochemical reactivity of the analogous fragment produced either in baculovirus-infected insect cells or in yeast. These results demonstrate that the positive effect of MBP in assisting the folding of passenger proteins extends to the correct formation of disulfide bridges in vivo. Although proteins or protein fragments fused to MBP have been frequently expressed with success, our comparative study evidences for the first time the helping property of MBP in the oxidative folding of a disulfide-rich protein.

Among the many systems available for heterologous protein production, the Gram-negative bacterium *Escherichia coli* remains the most attractive. Indeed, its ability to grow rapidly with inexpensive substrates enables one to obtain large amounts of biomass at a very low cost. There is, however, no guarantee that expression of a recombinant heterologous gene in *E. coli* will lead to accumulation at high levels of the corresponding protein in its native fold. In vivo misfolding often leads to aggregation into inclusion bodies or to proteolytic degradation. Production of heterologous disulfide-bridge containing proteins is particularly difficult since in such cases, the native conformation is generally conditioned by the correct arrangement of the disulfide bonds. It has been observed that expressing the protein of interest as a hybrid protein with a fusion partner can improve its production and solubility (*1*) (e.g., by protecting the passenger protein from proteolysis). For example, some proteins that form inclusion bodies when expressed in bacteria become soluble when produced as fusion proteins with the *E. coli* maltose-binding protein (MBP)[1] (*2*−*4*), and recently, this property has been used within the context of the structural genomic project (*5*). However, producing a heterologous multidisulfide bridged protein in its native conformation in *E. coli* remains a challenge. Indeed, disulfide bonds cannot be formed spontaneously in the cytoplasm because of its reducing potential. This difficulty was encountered while trying to produce, in the periplasm of *E. coli*, the natively folded carboxyterminal domain of the merozoite surface protein (MSP-1) from *Plasmodium falciparum*, a fragment of about 100 residues, containing six disulfide bridges. In the parasite, MSP-1 is synthesized as a 195 kDa precursor, located on the surface of the merozoite, the erythrocyte-invasive form. MSP-1 undergoes a proteolytic processing during schizonte rupture and merozoite invasion, leaving the C-terminal polypeptide, the so-called F19 fragment, attached to the merozoite membrane by a glycosyl-phosphatidylinositol (GPI) anchor (*6*). The F19 fragment is a promising malaria vaccine candidate (*7*). It is the target of a series of monoclonal

† This work was supported by funds from the Institut Pasteur, the CNRS (URA 2185), and the Ministère de l'Education Nationale, de la Recherche et de la Technologie.

* To whom correspondence should be addressed. Tel.: (+33)-145688387. Fax: (+33)140613043. E-mail: planson@pasteur.fr.

‡ Unité de Repliement et Modélisation des Protéines.

§ Unité de Résonance Magnétique Nucléaire des Biomolécules.

[1] Abbreviations: CD, circular dichroism; EGF, epidermal growth factor; F19, C-terminal fragment of MSP-1; F19bac, F19cytopl, F19fus, and F19isol: F19 fragment expressed in insect cells transfected with baculovirus, in *E. coli* cytoplasm, and in *E. coli* periplasm fused to MBP or without a fusion partner, respectively; MBP, maltose binding protein; MBP-F19fus, fusion protein of MBP and F19fus; MSP-1, merozoite surface protein 1; NBT/BCIP, nitro blue tetrazolium/5-bromo-4-chloro-3-indolyl phosphate; nOe, nuclear Overhauser effect; NOESY, nuclear Overhauser effect spectroscopy; PBS, phosphate buffer saline; PGSLED, pulse-field gradient stimulated-echo longitudinal encode−decode experiment; TOCSY, total correlation spectroscopy.

10.1021/bi035321c CCC: $25.00 
Published on Web 10/21/2003

antibodies able to inhibit the invasion of red blood cells in vitro (*8*, *9*). The native structure of F19 has been established by NMR (*10*) and X-ray (*11*) using recombinant proteins expressed in yeast and in insect cells, respectively. The structure consists of two epidermal-growth-factor (EGF) like domains, rich in antiparallel $\beta$-sheets. Each EGF domain contains three disulfide bridges, and the large interface between the domains is formed by a cluster of hydrophobic residues. Immunoreactivity studies with sera of malaria-immune individuals and vaccination tests on primates, using the F19 fragment from *P. falciparum* related species (*Plasmodium vivax* and *Plasmodium cynomolgi*), have shown that the conformation of F19, and particularly the formation of the disulfides, is critical for the elicitation of protective antibodies in vivo. Preliminary unpublished studies performed in our laboratory indicated that, when produced in the cytoplasm of *E. coli*, the F19 polypeptide is soluble and does not form inclusion bodies. Analytical centrifugation studies showed it to be essentially monomeric (unpublished results), but SDS−PAGE in the absence or presence of reducing agent pointed to the absence of intra- as well as intermolecular disulfide bonds. Furthermore, the far-UV−CD spectrum of the polypeptide chain obtained in the cytoplasm was typical of a random coil and showed no evidence of secondary or stable tertiary structure. All attempts to perform oxidative folding of F19 in vitro under a large array of experimental conditions (in the presence of mixtures of reduced and oxidized glutathione at various concentrations, in the presence or absence of folding adducts such as urea or nondetergent sulfobetaines, and at various pHs ranging between 6 and 9 and temperatures between 4 and 37 °C) failed to produce native F19 and resulted in the appearance of either nonfolded protein or of aggregates (unpublished results). We therefore thought of expressing the F19 polypeptide chain in the periplasm, which, in addition to having a redox potential that favors the formation of disulfide bonds, contains proteins such as the thiol oxidase DsbA and the disulfide isomerase DsbC that can assist the formation and rearrangement of disulfides during protein folding.

Expression of F19 in the periplasm of *E. coli* was performed using two strategies. In the first approach, F19 was directly addressed to the periplasm by fusing it with the MBP signal peptide. The second approach consisted in constructing a hybrid protein containing F19 fused at the carboxyterminal end of MBP. This construct contains the MBP signal sequence at its aminoterminal extremity. A cleavage site specific for factor Xa was inserted between the two fusion partners. The final F19 fragments obtained from these constructs are hereafter named F19isol and F19fus, respectively. The expression products were purified, and the structure and immunoreactive characteristics of the resulting F19 fragments were analyzed. The native F19 fragment produced in insect cells, or in yeast, was used as a reference to compare their structural and immunochemical properties. This study evidences that MBP can efficiently assist the in vivo oxidative folding of a small heterologous disulfide-rich protein.

## MATERIALS AND METHODS

*Strains and Growth Media.* PM9 cells (*recA1 supE44 endA1*, *hsd R17*, *gyr A96*, and *Thi* Δ*(lac-proAB)* Δ*malE444*; gift from J. M. Betton, Pasteur Institute) were used as recipient cells for DNA manipulation. Strain NS2 (*12*), which is *malE* deficient and *degP*$^-$, was used for protein expression. Transformation of PM9 and NS2 cells was performed according to the protocol of Chung et al. (*13*). Luria−Bertani and 2YT media (*14*) were used for cell growth and protein expression.

*Plasmids.* The F19 nucleotide sequence was amplified by PCR from the plasmid PFsig19HisExt (gift from I. Holm, Pasteur Institute). The primers 5′ATAAGCTTAACATCTCGCAGCACCAATG3′ and 5′TAAGATCTTTATTAATGGTGATGGTG3′ were used for the F19isol construct. These contain the restriction sites for HindIII and BglII, respectively. For the MBP-F19fus construct, the primer pair used was 5′ATGAATTCAACACGATCATCTCGAAATTG3′ and 5′TATCTAGATTATTTGCTGCAGAAGATGCCGTCG-3′. The latter primers contain the restriction sites EcoRI and XbaI, respectively.

The amplified F19isol and F19fus sequences were subcloned into the sequencing plasmid PCRScript (Stratagen), from which the sequences were checked. The resulting plasmids, named PCSF19isol and PCSF19fus, were digested by the restriction enzymes HindIII and BglII (PCSF19isol) or EcoRI and XbaI (PCSF19fus). After digestion, the F19 sequences were subcloned into an expression vector linearized by the corresponding restriction enzymes. The F19isol sequence was inserted in the pT1H plasmid (*15*) in frame with the MBP signal sequence. The F19fus sequence was inserted into the plasmid pMalp (New England Biolabs Inc.), which encodes for MBP preceded by its signal sequence and followed by the cleavage site for factor Xa.

*Protein Expression.* The proteins resulting from these constructions are F19isol and MBP-F19fus. F19isol contains a polyhistidine extension at the C-terminus and one cloning residue (K) at the N-terminus. The sequence of F19 in F19isol starts at residue $^{1612}$L of MSP-1 (*16*). MBP-F19fus is a fusion of MBP and F19, which contains the cleavage site for factor Xa. The sequence of F19, which starts at residue $^{1597}$N of MSP-1, is 15 residues longer than in F19isol. It also contains nine residues following the cleavage site for factor Xa at the N-terminus and a lysine residue at the C-terminus. The same protocol was used for expression of both proteins. NS2 cells were grown at 30 °C in 2YT medium supplemented with 0.1 mg/mL ampicillin. Expression was induced by 1 mM IPTG at $OD_{600} = 0.6$ and was carried out during ca. 2 h until the turbidity of the culture reached an $OD_{600} = 2.0$.

*F19isol Purification.* After cell harvesting, the periplasmic material was isolated with 1 mg/mL polymyxine B sulfate (ICN) in buffer A (20 mM sodium phosphate, 500 mM NaCl, pH 7.4) supplemented with 20 mM imidazole, followed by a centrifugation at 30 000*g* for 20 min at 4 °C. F19isol was purified using a HI-TRAP-Ni column (Pharmacia) preequilibrated in buffer A plus 20 mM imidazole. After loading, the column was washed with buffer A supplemented with 60 mM imidazole. F19isol was eluted with 500 mM imidazole in buffer A.

*Purification of MBP-F19fus and Isolation of F19fus.* Cells were centrifuged, and the pellet was suspended in buffer B (20 mM Tris, 100 mM NaCl, pH 8.0) supplemented with 1 mg/mL polymyxine B sulfate to isolate the periplasmic material. The soluble periplasmic fraction, obtained after centrifugation at 30 000*g* for 20 min at 4 °C, was passed

through an amylose agarose column (New England Biolabs Inc). The column was preequilibrated with buffer B and washed with the same buffer after loading. The fusion protein MBP-F19fus was eluted with 10 mM maltose in buffer B.

The fusion protein was cleaved with factor Xa (New England Biolabs Inc.) at 1% (w/w) final concentration. Proteolysis was performed at 37 °C for 48 h in buffer B supplemented with 2 mM $CaCl_2$. Two affinity chromatographies were performed to purify F19fus. The sample was first passed through an amylose agarose column to remove MBP and uncleaved MBP-F19fus. The second step, which was used to remove the protease and residual MBP, was an immunoadsorption onto immobilized monoclonal antibody G17.12 (gift from F. Nato, Pasteur Institute). This antibody was raised against MSP-1 and recognizes specifically F19. The immunoadsorbent was equilibrated and washed with buffer B to avoid a supplementary dialysis. F19fus was eluted by 100 mM glycin pH 1.8. The eluted material was immediately neutralized with 1 M $K_2HPO_4$ (1:20 v/v).

*Preparation of the Immunoadsorbent.* The monoclonal antibody G17.12 was purified from ascitic fluids by an ammonium sulfate precipitation at 40% followed, after dialysis, by Hi-Trap Sepharose Q fast flow (Pharmacia) chromatography. The column was preequilibrated in 20 mM triethanolamine, pH 7.7. Immunoglobulins were eluted by a linear gradient from 0 to 1 M NaCl in 20 mM triethanolamine pH 7.7. The collected antibody was coupled to CNBr-activated Sepharose 4B (Pharmacia), according to the protocol recommended by the supplier.

*Protein Concentration.* Protein concentrations were determined by absorbance using a molar extinction coefficient at 280 nm of 70 080 $M^{-1}$ $cm^{-1}$ for MBP-F19fus, and 3730 $M^{-1}$ $cm^{-1}$ for F19isol and F19fus. Extinction coefficients were estimated from sequence (*17*).

*SDS−PAGE and Immunoblot Analysis.* Electrophoresis was performed in the presence or absence of 2-mercaptoethanol in the denaturing buffer. SDS−PAGE containing 13.5% acrylamide was carried out according to the method described by Laemmli (*18*) and stained with either Coomassie blue or silver nitrate (*19*). Western blots were performed to reveal the presence of MBP-F19fus, F19fus, and F19isol. The anti-F19 antibody concentration was 1 $\mu$g/mL. Anti-mouse G immunoglobulins from goat, conjugated to alkaline phosphatase (Promega), were used as the second antibody. Bands were visualized by means of the NBT/BCIP reaction.

*ELISA.* The method of Friguet et al. (*20*) was used for determining the equilibrium association constant of antigen−antibody interactions in solution with four different monoclonal antibodies. Immunoglobulins were provided by F. Nato (Pasteur Institute). The antigens were MBP-F19fus, F19isol, and F19cytopl (F19cytopl was kindly provided by I. Holm and S. Longacre, Pasteur Institute). The latter F19 fragment, produced in the cytoplasm of *E. coli*, has no disulfide bridge. ELISA plates were coated overnight at 4 °C with 100 $\mu$L per well of the 1 $\mu$g/mL antigen (MBP-F19fus) solution in 50 mM $NaHCO_3$ pH 9.6. No interaction between antibodies and MBP was detected under these conditions. The antibody concentration ($9 \times 10^{-11}$ M) was established according to the validation criteria reported by Friguet et al. (*20*) to ensure the linearity of the absorbance readings versus the free antibody concentration and to avoid a significant readjustment of the equilibrium in the liquid phase during the incubation (7 min) of antigen−antibody mixtures in the coated wells. Anti-mouse IgGs conjugated to alkaline phosphatase were used as secondary antibodies at a 1:7500 dilution. Detection at 405 nm was performed using *p*-nitrophenyl phosphate tablet sets (Sigma). Each affinity determination was independently repeated at least twice, and in all experiments, antigen concentration was tested in quadruplicate.

*N-Terminal Sequencing.* After electrophoresis, the proteins were electrotransferred onto a poly(vinylidene difluoride) membrane (4 h at 40 mA). After staining with 0.1% Amido Schwarz in 40% methanol and 1% acetic acid, the bands of interest were cut and submitted to microsequencing. Edman degradation was carried out with an Applied Biosystems Procise sequencer (microsequencing technical platform, Pasteur Institute) for F19fus and F19isol preparations, respectively.

*Mass Spectrometry.* Mass determination experiments were run at the mass spectrometry technical platform of the Pasteur Institute. Samples were dissolved in water/methanol/formic acid (50:50:5) and were introduced into an API365 triple−quadrupole mass spectrometer (AB-MDS-Sciex, Thornill, Canada) at 5 $\mu$L/min with a syringe pump (Harvard Apparatus, South Natick, MA). The device was equipped with an atmospheric pressure ion source used to sample positive ions produced from a pneumatically assisted electrospray interface.

*Circular Dichroism.* Far-UV circular dichroism spectra were acquired on a CD6 Jobin-Yvon spectropolarimeter between 180 and 260 nm at a 2 nm constant bandwidth with a 0.5 nm step and an integration time of 5 s. Samples (1 mg/mL) were dialyzed against 50 mM ammonium bicarbonate before recording the spectrum. A 0.01 cm circular cell was used. Five successive scans were averaged. The baseline was acquired on dialysis buffer under the same conditions and subtracted from the sample spectrum. Quantitative secondary structure composition was determined from the resulting spectrum after normalization, using the variable selection decomposition program (Varselec) from Manavalan and Johnson (*21*).

*NMR.* NMR samples of F19fus and F19isol were prepared by dissolving freshly lyophilized protein in 20 mM deuterated ($d_3$) sodium acetate, pH 4.0 (buffer C), 10% $D_2O$. Samples were centrifuged at 17 600*g* for 30 min at 4 °C to remove any possible high molecular weight aggregate. The concentration was 0.4 mM for both proteins.

NMR experiments were performed at $^1H$ resonant frequencies of 499.8 or 599.9 MHz on Inova spectrometers (Varian Inc., Palo Alto, CA) equipped with gradient probes. The sodium salt of 4,4-dimethyl-silapentane (DSS) was used as an external reference for chemical shifts. Data were acquired, processed, and analyzed on Sun Ultra stations using Vnmr 6.1C (Varian Inc.) and NMRView 5.0.3 (*22*).

NOESY (*23*) and TOCSY (*24*, *25*) spectra were acquired at 35 °C with 2048 data points in the direct dimension, 256 $t_1$ increments, and 48 or 72 transients per $t_1$ increment. Spectra were recorded using a spectral window of 12 ppm and a recycling delay of 2.0 or 2.2 s. Solvent suppression was achieved by means of the watergate pulse scheme (*26*, *27*). Mixing times in NOESY and TOCSY experiments were 120 and 70 ms, respectively.

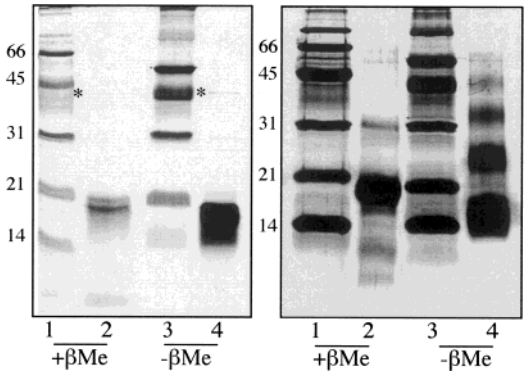


FIGURE 1: SDS gel electrophoresis of F19 in the presence or absence of 2-mercaptoethanol ($\beta$Me). Gels were stained with silver nitrate. Left panel, lanes 1 and 3: low-range molecular weight markers (Biorad) and lanes 2 and 4: F19fus (7.5 $\mu$g). Right panel, lanes 1 and 3: low-range molecular weight markers (Biorad) and lanes 2 and 4: F19isol (7.5 $\mu$g). *: residual MBP. Molecular weights (kDa) are indicated.

The diffusion coefficient of F19fus was determined by pulse-field gradient spin−echo NMR using the PGSLED sequence (*28*). The encode−decode gradients were applied on the *x* axis to minimize eddy currents. Five independent experiments were performed on a protein sample with buffer C prepared in $D_2O$. A small amount of dioxan (0.05% final concentration) was added to the sample as a radius standard. The apparent diffusion coefficient of the protein was used to calculate its Stokes radius as described in ref *29*.

## RESULTS

*Isolation and Characterization of F19isol.* To examine the periplasmic expression and folding of F19, the fragment was fused to the MBP signal peptide. Following the induction of expression, the fragment accumulated in the periplasmic space as a soluble protein.

The N-terminal amino acid sequence of the purified fragment is KLNIS, which is the expected F19 N-terminus after in vivo cleavage of the signal peptide. The ESI-MS spectrum shows a single peak corresponding to a molar mass of 11396.8 ± 0.3 Da, which is effectively identical to the expected mass for the fully oxidized protein (11396.6 Da) and indicates that no proteolytic degradation occurred at the C-terminal end of the fragment. SDS−PAGE gels (Figure 1, right panel) obtained under reducing conditions show a major band corresponding to the expected molar mass of the polypeptide chain. Under nonreducing conditions, the electrophoretic profiles display a major band that corresponds to the monomer, along with other bands which may correspond to covalently linked oligomers not detected by mass spectrometry.

The conformation of the F19isol fragment produced in the *E. coli* periplasm was probed using four monoclonal antibodies, which recognize the F19 fragment obtained from insect cells (F19bac). Equilibrium association constants of antigen−antibody interactions in solution were determined by ELISA using the competition method described in the Materials and Methods. The affinity constants of the four antibodies for F19bac, which is natively folded as established by X-ray crystallography (*11*), were taken as reference (F. Nato, Pasteur Institute, unpublished results).

As shown in Figure 2, F19isol shows a much lower affinity than F19bac for the four antibodies (Table 1). This indicates that F19isol adopts a conformation different from that of F19bac and/or that only a small fraction of the F19isol molecules presents the epitopes of F19bac.

As a control, the association constants of a reduced form of F19 obtained from cytoplasmic expression in *E. coli* were determined. As shown in Figure 2 and Table 1, this species is poorly recognized by three of the four antibodies. Noteworthy, except for antibody G17.12, for which a coincidence of the binding curves for F19isol and reduced F19cytopl was observed, there is no correlation between the immunoreactivities of the two antigen forms. This observation suggests that these species adopt different conformations. This could be expected since in F19cytopl no disulfide bridge is present, whereas F19isol is fully oxidized as shown by ESI-MS analysis.

In summary, F19 produced as an isolated protein in the periplasmic space is unable to fold correctly. Mass spectrometry indicates that all the cysteines of F19isol are engaged in disulfide bonds. Hence, the different immunoreactivity displayed by F19isol as compared to F19bac suggests that at least some, if not all, of its cysteines are mispaired.

The secondary structure composition of F19isol was established from the corresponding far-UV circular dichroism spectrum (Figure 3). As shown in Table 2, singular value decomposition of the spectrum of F19isol using the Varselec program (*21*) indicates the presence of 23% of extended $\beta$-strands. This value is somewhat lower than that calculated from the NMR (28%, ref *10*) and X-ray structures (30%, G. Bentley, Pasteur Institute, private communication) of recombinant F19 produced in yeast and in insect cells, respectively. Moreover, the sum of structural fractions (82%) is far from the expected value of 100%. This indicates that, unlike that of F19fus (see next), the CD spectrum of F19isol is not well-described by the CD spectra of the Varselec database. The previous results suggest that when expressed in the periplasm of *E. coli*, F19 does not possess all the characteristics of the native conformation.

*Isolation and Characterization of F19fus.* The strategy consisting in using protein fusions has been frequently used to produce heterologous proteins in their native state. Assuming a putative role of MBP in controlling the folding process of a passenger protein, we decided to apply this strategy and fused F19 to the C-terminal extremity of MBP. Periplasmic expression was ensured by keeping the signal peptide of MBP. Isolation of the F19 fragment was made possible by the presence of a cleavage site specific for the factor Xa protease. To facilitate the proteolysis, the F19 moiety (119 residues) included 16 N-terminal residues belonging to its natural precursor and known to be excised by baculovirus-infected insect cells (G. Bentley, V. Chitarra, and S. Longacre, Pasteur Institute, personal communication).

Upon induction, the fusion protein MBP-F19fus was found in the periplasmic space as a soluble protein. After purification, the fusion protein was submitted to proteolysis by factor Xa. F19fus was further purified by affinity chromatography, first on an amylose agarose column to eliminate residual MBP and uncleaved fusion protein, and then on immobilized G17.12 monoclonal antibody to eliminate the protease. The resulting F19fus was found to be soluble after isolation. Figure 1 (left panel) shows the electrophoretic profiles of the purified F19fus fragment obtained after SDS denaturation with and without 2-mercaptoethanol. The preparation appears

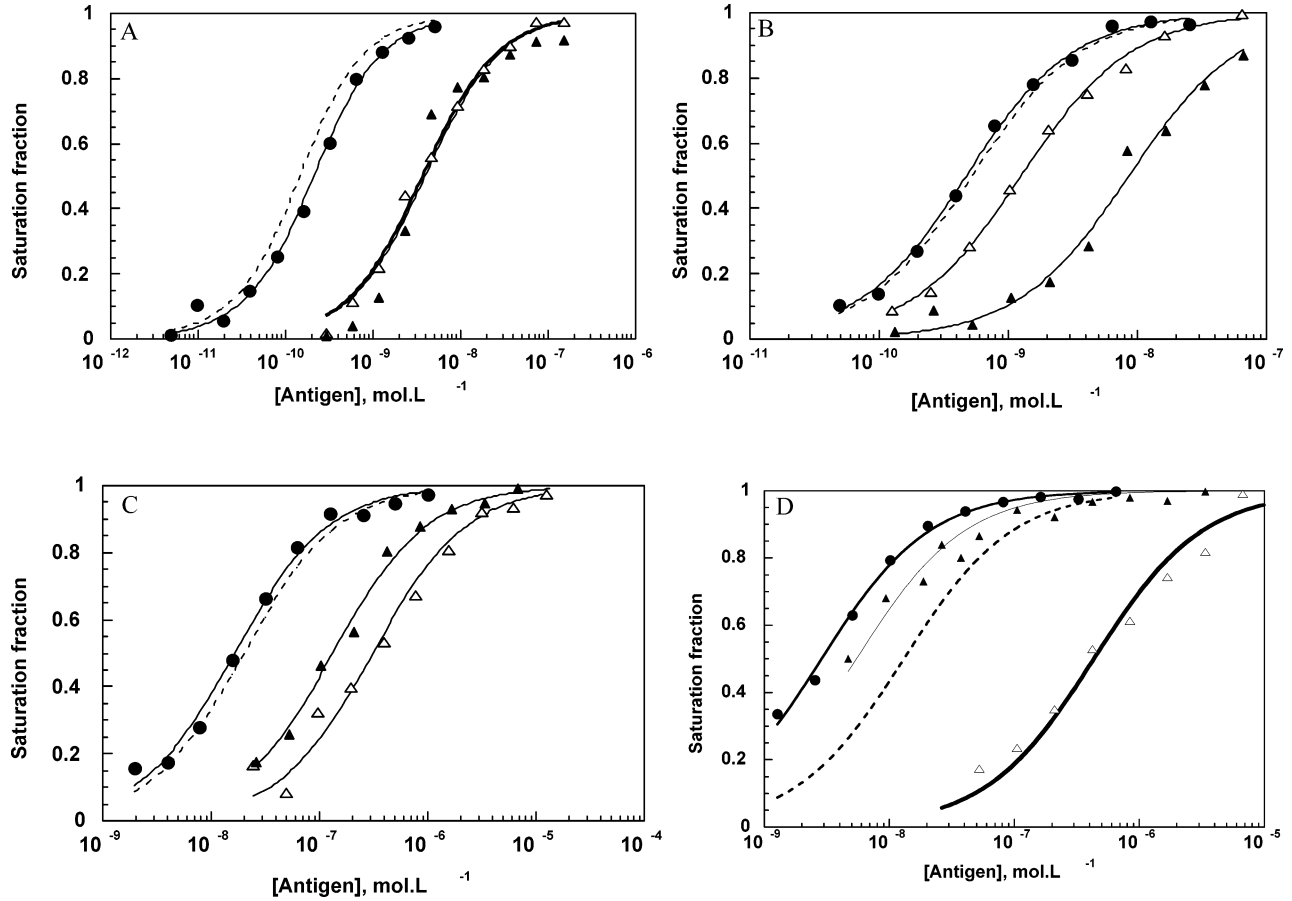


FIGURE 2: Determination of affinities of F19 toward monoclonal antibodies. Binding of antibodies G17.12 (A), A8.1 (B), D11.4 (C), and D12.8 (D) to F19 fragments. - - -: F19bac; ●: MBP-F19fus; △: F19isol; and ▲: F19cytopl. Binding curves (solid lines) were established from the fit of the data to the equation $\left(Ab_0 + Ag_0 + K_D - \sqrt{(Ab_0 + Ag_0 + K_D)^2 - 4Ab_0Ag_0}\right)/2Ab_0$, where $Ag_0$ and $Ab_0$ represent antigen and antibody total concentrations respectively, and $K_D$ is the equilibrium dissociation constant. The binding curves corresponding to F19bac (dashed lines) were simulated using the same equation and the corresponding equilibrium constants (F. Nato, unpublished results).

Table 1: Solution Equilibrium Association Constants of F19−Antibody Interactions[a]

| antibodies | F19bac | MBP-F19fus | F19isol | F19cytopl |
|---|---|---|---|---|
| G17.12 | $10^{10}$ | $6.25 \times 10^9$ (0.66) | $2.8 \times 10^8$ (0.03) | $2.6 \times 10^8$ (0.03) |
| A8.1 | $2.1 \times 10^9$ | $2.3 \times 10^9$ (1.29) | $7.7 \times 10^8$ (0.37) | $1.1 \times 10^8$ (0.05) |
| D11.4 | $5 \times 10^7$ | $7.1 \times 10^7$ (1.52) | $3.3 \times 10^6$ (0.07) | $7.7 \times 10^6$ (0.15) |
| D12.8 | $7.7 \times 10^7$ | $3.1 \times 10^8$ (4.42) | $2.3 \times 10^6$ (0.03) | $1.6 \times 10^8$ (2.08) |

[a] The association constants ($K_A$) were determined at 25 °C in PBS-Tween buffer pH 7.4 supplemented with 0.02% bovine serum albumin. $K_A$ values are expressed in $M^{-1}$. The experimental error represents 10−20% of the corresponding $K_A$ value. The ratio of the association constants between an F19 fragment and the F19bac is given in parentheses.

almost completely exempt of free residual MBP. In nonreducing conditions, the fragment migrates as a broad band. In the presence of reducing agent, the fragment migrates as a doublet when the gel is silver stained and as a diffuse band when the gel is stained with Coomassie blue (data not shown). That F19fus migrates at the expected position for a monomer of the size of F19 under nonreducing conditions indicates that no intermolecular disulfide bonds are formed.

Microsequencing of the 11 N-terminal amino acids was in agreement with the expected sequence and indicated that cleavage with factor Xa was homogeneous. It is important to mention that only one amino acid derivative was detected in each step of the Edman degradation, which suggests that F19fus samples are chemically homogeneous. Noteworthy, F19fus contains an N-terminal extension of 25 residues relative to the sequence of F19 previously used for structure determination (*10*, *11*) (see Materials and Methods for details). ESI-MS revealed a single species with a molar mass of 13266.7 ± 0.7 Da. This value is in agreement with the expected mass (13 265.8 Da) of the single component detected by microsequencing with its 12 cysteine residues engaged in disulfide bridges. The coincidence between the expected and the observed molar masses proves that the F19 fragment did not undergo any proteolysis. From the analysis of silver stained SDS−PAGE gels, N-terminal sequencing, and mass spectrometry, it can be concluded that F19fus samples are highly pure and chemically homogeneous and that the F19fus fragment contains six disulfide bridges.

As in the case of F19isol, we examined the immunoreactivity of F19fus using the same four monoclonal antibodies and experimental procedures. Since no cross-reactivity between MBP and four antibodies was detected, the immunoreactivity of F19fus was measured using the MBP-F19fus fusion protein as antigen. As shown in Figure 2, the binding

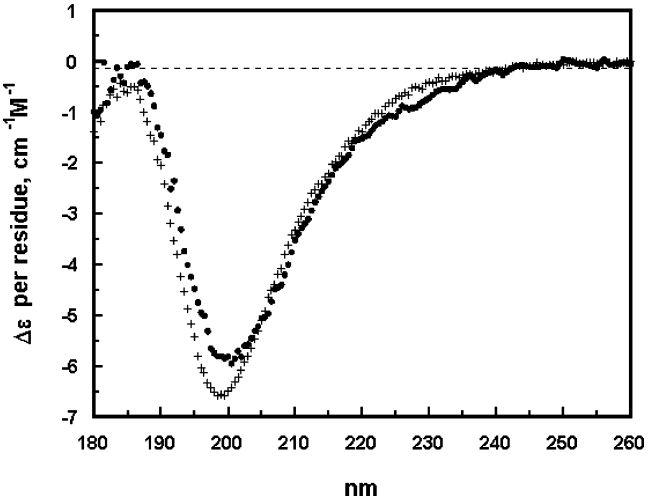


FIGURE 3: Far-UV circular dichroism spectra of F19fus and F19isol. +: F19fus and ●: F19isol. Each spectrum corresponds to the average of five successive acquisitions. The spectrum of buffer acquired under the same conditions was subtracted. For detailed experimental conditions, see the Materials and Methods.

Table 2: Secondary Structure Composition of F19 Fragments Produced in Yeast, Insect Cells, and *E. coli*[a]

| | Nb residues | % α | % β | % others | sum |
|---|---|---|---|---|---|
| F19 yeast (NMR) | 93 | 0 | 28 | 72 | 100 |
| F19bac (X-ray) | 93 | 7 | 30 | 63 | 100 |
| F19fus (CD) | 119 | 6 | 27 | 67 | 100 |
| F19isol (CD) | 101 | 5 | 23 | 54 | 82 |

[a] The secondary structure contents of F19yeast and F19bac were determined from the NMR (*10*) and the X-ray (G. Bentley, private communication) structures, respectively, using the software MOLMOL 2k.1 (*40*), and taking into consideration only the 93 residues common to the two constructs. The CD spectra of F19fus and F19isol shown in Figure 3 were deconvoluted in terms of secondary structure content using the singular value decomposition method with a variable selection of CD spectra as implemented in the Varselec program (*21*).

curves corresponding to MBP-F19fus are almost coincident with those corresponding to F19bac, except in the case of antibody D12.8 for which the former displays a significantly higher affinity (Table 1). To summarize, the epitopes of F19bac specific for the four monoclonal antibodies are present in F19fus.

To further explore the conformational properties of F19fus, its far-UV CD spectrum (Figure 3) was analyzed using the Varselec program (*21*). As shown in Table 2, singular value decomposition of the spectrum of F19fus indicates the presence of 27% of extended β-strands, a value very close to that deduced from the NMR (*10*) and X-ray structures (G. Bentley, Pasteur Institute, private communication) of recombinant F19 produced in yeast and in insect cells. Furthermore, as opposed to the CD spectrum of F19isol, the CD spectrum of F19fus can be correctly represented with the database included in Varselec, as indicated by the 100% value of the sum of the α, β, and irregular (other) structures (Table 2).

*NMR.* Taking into consideration the apparent difference in conformation between F19isol and F19fus, we recorded TOCSY and NOESY $^1$H NMR spectra of the two fragments and compared them to spectra obtained for F19bac under the same experimental conditions (J. I. Guijarro, V. Chitarra, S. Longacre, G. Bentley, and M. Delepierre, unpublished data). These spectra, especially the NOESY experiment, which shows dipolar (through space) connectivities between atoms that are less than 5 Å apart, provide a detailed fingerprint of the structure of a given protein in solution.

Two-dimensional spectra of F19isol show broad signals, very poor dispersion of chemical shifts (δ), and a low number of signals relative to what is expected for a globular structured protein of ∼100 residues (Figure 4A). For comparison, the NOESY spectrum of the globular and natively folded F19bac is included in Figure 4B. Moreover, in the NOESY spectrum of F19isol, there is no nOe characteristic of stable regular secondary structures (sheets, helices, or turns) in the HN−HN region. All these features are typical of an unfolded or poorly folded protein. In addition to these signals arising from an unfolded/partly folded molecule, there are several weak signals that are well-resolved and that may arise from a low-populated structured conformer. The latter signals are sharper and show a greater dispersion of chemical shifts. Some of these weak peaks correspond to Hα or HN protons with downfield shifted resonances ($\delta \geq 5$ or $\geq 8.6$ ppm, respectively). These downfield shifts are typically observed for protons involved in β-sheets or turns. Moreover, the well-resolved sharp signals can be superimposed to signals in the equivalent spectra of F19bac, indicating that this low-populated conformer ensemble has, at least locally, the same structure as F19bac. From the relative intensity of some of these well-resolved signals in the one-dimensional spectrum of F19isol, the population of this structured conformer ensemble can be estimated to be roughly 5%.

F19fus spectra contain two distinct sets of resonances. On one hand, the spectra display low-intensity broad signals that are clustered in regions corresponding to chemical shifts of protons in unfolded proteins. For instance, a cluster of broad signals can be observed in the NOESY spectrum of F19fus centered at ∼8.3 ppm (F2 dimension) and ∼4.4 ppm (F1 dimension) (see Figure 4C). These correspond to dipolar interactions between HN and Hα protons, respectively, that resonate at the so-called random coil chemical shifts. On the other hand, F19fus spectra show much sharper signals with a good dispersion of chemical shifts, which is indicative of a folded protein. Moreover, the downfield shift (higher ppm values) of many Hα and HN resonances relative to the random coil values ($\delta \geq 5$ or $\geq 8.6$ ppm, respectively), and the presence of strong Hα−HN and weak HN−HN correlations in the NOESY spectrum, are indicative of β-sheet structures. The existence of Hα−Hα correlations in the NOESY spectrum of F19fus acquired in $D_2O$ (not shown) further indicates that at least some of the β-sheet structures are antiparallel, in agreement with the high content of antiparallel β-sheets determined for F19bac from crystallographic data.

A careful and detailed comparison of the spectra of F19fus and F19bac was performed. It should be mentioned that these constructs have a different length and different termini. Indeed, F19fus (119 residues) contains 25 extra N-terminal residues relative to F19bac, which in turn, displays a six-residue C-terminal histidine tag, absent in F19fus. If the broad signals mentioned previously are not taken into account, and if one allows for sequence differences at the N- and C-termini of the fragments and differences in sensitivity and in water suppression, the spectra of both F19

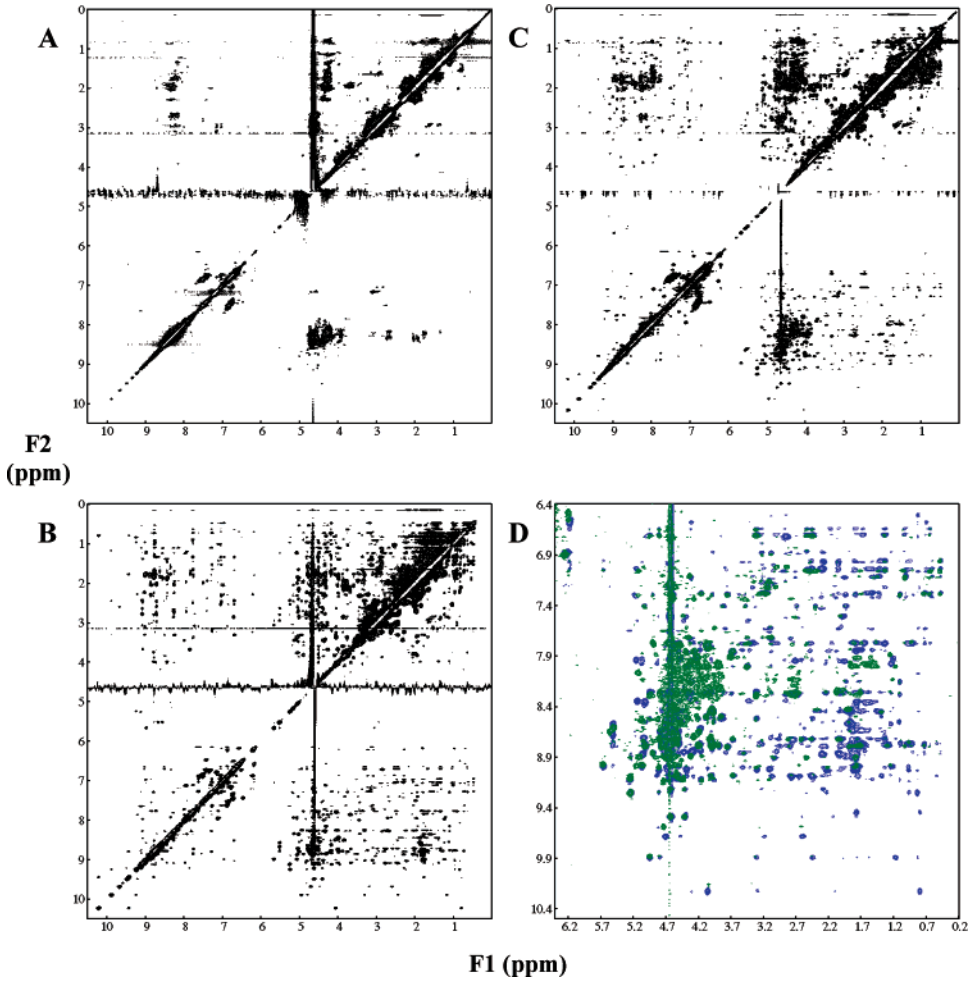


FIGURE 4: NOESY spectra of F19isol, F19bac, and F19fus. The spectra were acquired at 35 °C. The protein samples were dissolved in 20 mM CD3COONa, 10% $D_2O$, pH 4.0. (A) F19isol (0.4 mM); (B) F19bac (1.2 mM); (C) F19fus (0.4 mM); (D) Superposition of the fingerprint region of the NOESY spectra of F19fus (green) and F19bac (blue). Concentrations were 0.4 mM for F19isol and F19fus and 1.2 mM for F19bac.

fragments superimpose very well (see Figure 4D). Moreover, on the basis of the published chemical shifts of the F19 fragment obtained from yeast and used for structure determination by NMR (*10*), focusing on well-resolved HN resonances, and using through-bond and intra- and interresidue through-space connectivities, it was possible to unambiguously assign signals in F19fus (and F19bac) TOCSY and NOESY spectra for 19 different residues: Q6, C7, V8, Y34, K35, E51, N52, G54, K61, C62, T63, I74, T75, E77, C78, G89, I90, F91, and S93, in F19bac numbering. The TOCSY and NOESY signals of these residues in F19fus spectra superimpose very well with signals of F19bac. This clearly indicates that these residues are implicated in exactly the same structures in F19fus and F19bac. These residues are spread throughout the entire sequence and structure of F19. Importantly, the signals of three cysteine residues (C7, C62, and C78) involved in three different disulfide bridges located in both EGF domains, of residues contiguous to the latter cysteines (Q6, V8, T63, and E77), and of residues I90 and F91, located in the hydrophobic core at the interface of the EGF modules, were assigned. Taken together, all these results unambiguously demonstrate that the F19fus preparation contains a high proportion of globular and totally natively folded molecules with correct disulfide bonds.

The broad signals observed in F19fus spectra could be either due to (i) an unstructured/partly folded N-terminus, (ii) to a population of nonorganized conformers, or (iii) to a combination of both possibilities. Importantly, the one-dimensional and two-dimensional $^1H$ spectra of two different samples of F19fus obtained from different expression/purification batches were undistinguishable. In particular, in one-dimensional spectra, in which the integral of a signal reflects the number of protons that contribute to it, the relative integrals of signals arising from the native protein and of signals in regions where the broad signals are clustered, are the same. This observation suggests that the atoms that give rise to the broad signals are born by the same molecules that produce the native signals, as it is very unlikely that two different expressions/purifications would lead to exactly the same proportion of native/non-native molecules.

To further assess whether F19fus samples contain two conformationally distinct populations of molecules, or not, NMR diffusion experiments were performed as described by Wilkins and collaborators (*29*). In principle, if folded and unfolded molecules with a different hydrodynamic volume coexisted in the same sample, the latter experiments should distinguish between them. The sample of F19fus used for NMR experiments in buffer C prepared in $H_2O$ was freeze-

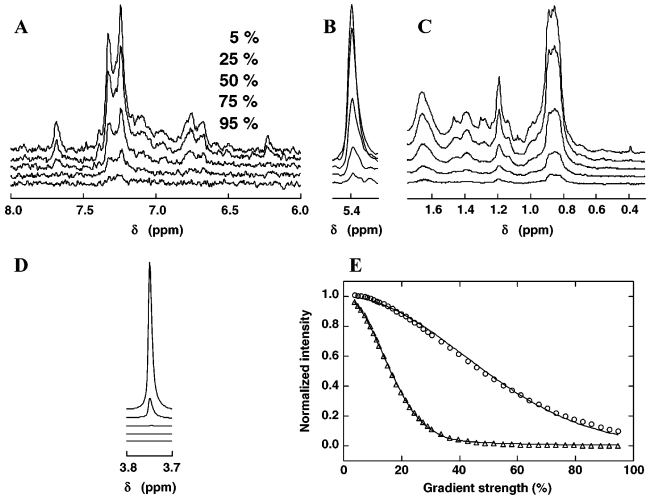


FIGURE 5: NMR translational diffusion experiments. The experiments were performed at 25 °C with F19fus dissolved in 20 mM CD3COONa, 100% $D_2O$, pH 4. (A−D) Regions of the PGSLED $^1H$ spectra of F19fus recorded using different pulse-field gradient strengths as indicated in the figure. (A) Low-field region; (B) signal of an Hα proton of the natively folded protein; (C) upfield region; and (D) signal of dioxan, which is used as an internal diffusion standard. For comparison purposes, the intensities of each region of the spectra are normalized relative to its most intense signal at a gradient strength of 5%. (E) Dependence of the integral (*i*) of the region shown in C for the protein (O) and in panel D for dioxan (Δ) on the strength of the field-gradient (*g*). Field-strength is expressed as a percentage of the maximum strength available (ca. 30 G $cm^{-1}$). Data were fit to Gaussian functions. F19fus data were fit to a single Gaussian function: $i = i_0 e^{-dg^2}$, where $i_0$ represents the intensity in the absence of gradients, and *d* is the apparent diffusion coefficient under the conditions used. Dioxan data were fit to a sum of two Gaussian functions as dioxan protons resonate at a frequency at which protons from the protein also resonate. From the apparent diffusion coefficients of dioxan and of the protein, and the known Stokes radius of dioxan (2.12 Å, see ref *29*), the hydrodynamic radius of the protein can be calculated.

dried and resuspended in $D_2O$. After the addition of a small amount of dioxan, which serves as a diffusion standard, the sample was used for pulse-field gradient spin−echo NMR experiments. As shown in Figure 5A−C, all the regions of the spectrum of F19fus display the same dependence on the field-gradient strength, while the signal of the small molecule dioxan (Figure 5D) vanishes much faster than the protein signals. It is interesting to note that the peak in Figure 5B, which arises from a downfield shifted Hα proton belonging to a β-sheet of the natively folded protein, shows the same apparent diffusion coefficient that the aromatic (Figure 5A) and aliphatic (Figure 5C) regions have. Hence, in terms of hydrodynamic size, the F19fus preparations seem homogeneous. The Stokes radius of F19fus was calculated from the fit to a Gaussian function of the dependence of the intensity of the protein signals on the applied field-gradient strength. The protein data fit well to a single Gaussian, with a Pearson correlation coefficient very close to unity (≥0.998). The Stokes radius was found to be 20.0 ± 0.5 Å, which is in agreement with the value expected for a monomeric globular protein of 119 residues (*29*). Data were also fit to a model in which two distinct populations exist (sum of two Gaussian functions), but although the fits also show a very good correlation coefficient, the obtained diffusion coefficients do not have a physical sense (data not shown). This further indicates that F19fus samples are homogeneous in hydrodynamic volume.

## DISCUSSION

Genetic recombination approaches are widely used to produce proteins with therapeutic interest in many expression systems. However, the production of recombinant proteins containing disulfide bridges remains difficult because of the stringent requirement of a correct coupling between folding and oxidation. Expression of such proteins is often achieved in eukaryotic systems, such as insect cells transformed with baculovirus, in which the oxidation of cysteines is made possible by exportation of the expression product to the culture medium. This procedure has been used with success for F19, but its cost is intrinsically high. Alternatively, the production of recombinant proteins in bacteria such as *E. coli* is much less expensive, but in the case of disulfide-rich proteins, the correct coupling between folding and oxidation is difficult to achieve. Genetic constructions addressing the gene product to the periplasm in principle allow formation of disulfide bonds because of the favorable redox potential of the periplasm. In addition, disulfide formation is assisted by thiol oxidase and disulfide isomerase, which favor conversion and interconversion of disulfide bridges. Nevertheless, both eukaryotic or prokaryotic approaches may fail due to misfolding induced by incorrect (non-native) pairing of disulfide bonds of the gene product.

In the present work, we tested the production of the F19 fragment in the *E. coli* periplasm as an alternative to the established expression procedures using insect cells or yeasts (*10*, *11*). This fragment of about a hundred amino acids contains six disulfide bridges. Its immunogenic and antigenic properties make it a highly valuable vaccine candidate against malaria. To assess whether the fragment produced in the *E. coli* periplasm can adopt the native conformation, it was expressed as the C-terminal partner of a fusion protein with MBP. This construction presented several advantages: (i) direct addressing to the periplasmic space due to the natural cellular localization of MBP; (ii) putative high solubility of the fragment helped by the high solubility of MBP; (iii) easy and rapid purification of the fusion protein using affinity chromatography with immobilized maltodextrin; and (iv) protection of the N-terminus from degradation by proteases. After cleavage of MBP and purification, the F19 fragment was found to be soluble. ES-MS revealed a chemically pure preparation with a molar mass corresponding to that of the fragment with its 12 cysteine groups oxidized. Deconvolution of the far-UV CD spectrum showed that the resulting F19fus fragment is folded with a secondary structure content close to that deduced from crystallographic and NMR data (Table 2). These characteristics could suggest that the sole exportation of the fragment into the periplasmic space might suffice to its correct oxidative folding.

F19 expressed as an isolated fragment (F19isol) fused to the signal sequence of MBP is also found in the periplasmic fraction as a soluble nondegraded protein. It has the expected molar mass with its 12 cysteines engaged in disulfide bridges. The quantitative analysis of its far-UV CD spectrum reveals the presence of mainly β-strands secondary structure but yields a sum of structural fractions of only 82%. The latter indicates that the CD spectrum of F19isol contains features

not represented in the native proteins database and suggests that the fragment preparation is not homogeneous. It is likely that this heterogeneity is due to mispairings of disulfide bridges that trap non-native conformations, and indeed, polymers stabilized by interchain disulfide bonds have been detected by nonreducing SDS PAGE. Such disulfide bridge scrambling has been evidenced in in vitro oxidative refolding of human EGF (*30*). In the case of F19, which consists of two EGF domains, trapped intermediates would be stable enough to resist catalyzed disulfide exchange. That F19isol contains a high proportion of non-native conformers was established by its comparative immunochemical reactivity toward four monoclonal antibodies and by NMR. Indeed, the affinities of F19isol for the monoclonal antibodies are substantially weaker than those of F19fus and of the homologous fragment produced in insect cells (F19bac) considered as a reference for the native format. In addition, NMR one- and two-dimensional NOESY and TOCSY spectra of F19isol are characteristic of a major species with no fixed tertiary structure and of a minor species (ca. 5%) of native or partially native molecules. Such states with fluctuating secondary structure have been described before (*31*, *32*). It may correspond to a molten or premolten globule-like state trapped by incorrect and heterogeneous pairing(s) of disulfide bridges.

From the previous results, it can be concluded that the two methods of production of recombinant F19 in the *E. coli* periplasm lead to different conformational states of the fragment. From its immunochemical reactivity, the fragment isolated from the fusion protein MBP-F19fus seems to have the native conformation, and its CD spectrum is consistent with the expected secondary structure. However, these results are not sufficient to assess if the preparations of F19fus are structurally homogeneous and totally native. We thus explored more precisely the structure of F19fus using $^1$H NMR spectroscopy. In contrast to F19isol NMR spectra, F19fus one- and two-dimensional spectra are characteristic of a structured molecule with a high content of antiparallel $\beta$-sheets. Comparison of the NMR spectra with those recorded with the homologous recombinant fragment produced in insect cells reveals a coincidence of a large number of resonances. Using reported chemical shift data of F19 produced in yeast (*10*), many of these resonances could be assigned to 19 residues spread along the amino acid sequence. These residues included three cysteines implicated in different disulfide bonds in both EGF domains and residues located in the hydrophobic core at the interface between the two EGF domains. This clearly indicates that a large proportion of F19fus adopts the native conformation consisting in two EGF domains, each stabilized by three disulfide bonds. However, NMR spectra of F19fus also show resonances typical of nonorganized conformations. These resonances could be interpreted as resulting from a population of unfolded molecules. However, NMR translational diffusion experiments indicate that F19fus is homogeneous in terms of hydrodynamic volume. Indeed, the diffusion data are well-described by an unimodal Gaussian function, and more importantly, all the regions of the spectrum of F19fus yield the same diffusion constant as a signal unambiguously assigned to the native protein. Moreover, the Stokes radius determined for F19fus (20 Å) is consistent with a folded compact molecule made of 119 residues (*29*). Finally, that two totally independent preparations of F19fus show the same NMR spectra, and the same relative intensity of native versus broad signals, also indicates that F19fus is homogeneous in terms of conformation. It is important to note that NMR results are in agreement with CD data as the latter indicate the same content of secondary structure for F19fus and the shorter fragments expressed in eucaryotes, suggesting that the N-terminal residues in F19fus are not structured, as shown by NMR. Taken together, these results show that the resonances corresponding to nonorganized residues result from the 25-residue N-terminal extension in F19fus that is not present in F19 produced in baculovirus or yeast.

In conclusion, we have succeeded in producing a disulfide-rich promising malaria vaccine candidate in its native state in *E. coli.* We also showed that periplasmic expression allows us to obtain the native conformation of a disulfide-bridge-rich protein when fused to the C-terminal extremity of MBP. Fusions with MBP have been successfully used to produce recombinant proteins in their native state in many cases (*33*−*36*). This has led to the idea that MBP can act as a molecular chaperone, in vivo (*1*) and in vitro (*37*). The chaperone effect of MBP (which is the prevention of aggregate formation) has been shown for a number of proteins that form inclusion bodies when expressed alone. However, a direct effect of MBP on the folding of a fusion partner has never been clearly demonstrated, and that is particularly true for a disulfide-rich protein. In the present study, by comparing the structure of the final states of a protein fragment containing six disulfide bridges expressed either individually or fused to MBP, we clearly show the assistance folding by MBP. We showed that periplasmic expression allows us to obtain the native conformation of a disulfide-bridge-rich protein when fused to the C-terminal extremity of MBP. This observation points out the assisting effect of MBP to the oxidative folding of the fusion partner. Whether this assisting effect on the folding of disulfide-rich proteins is a general property of MBP remains to be established. Indeed, this effect might be evidenced for some other proteins as passengers, which, when expressed as nonfused proteins, are soluble but have an incorrect folding. If not a general rule, the assisting property of MBP could depend on some compatibility or on reciprocal accommodation between the folding kinetics of both protein partners within the fusion. Additionally, this direct folding effect, distinct from the simple solubilization action, may not be specific of MBP as a partner within the fusion.

A direct assisting effect of MBP should at least involve transient interactions between the two fusion partners. It has been indeed reported that MBP can interact with its fusion partner and affect its stability (*38*, *39*). However, for disulfide-rich proteins, MBP cannot directly participate to the formation or to the breaking of disulfide bridges since its sequence does not contain any cysteine. Because in the case of F19, the fusion passenger when expressed alone is unable to intrinsically reach the native state, the helping role of MBP would be to orient its partner folding in a way that enables it to escape kinetic traps. This can be achieved by slowing down the early formation of disulfides, thus limiting the number of early intermediate populations with mispaired disulfide bridges and subsequently allowing a progressive sequential oxidative folding process. To our knowledge, no study of the role of MBP in the folding of a fused protein

has been described. Experiments to study in vitro the role of MBP on the folding of F19 and to determine if the folding of MBP is altered by the presence of F19 are underway to shed light on the mode of action of MBP.

Our study was focused on MBP because of its natural periplasmic localization and also because it has been previously shown that, as compared to other fusion partners, MBP had the higher solubilization effect for inclusion bodies. Therefore, we theorized that MBP might help the folding of F19. Proteins other than MBP could be tested as partners for F19 with the aim of showing whether they exhibit a folding assisting effect. Such a study could show that a variety of fusion partners can have the same effect as MBP, thus extending the range of fusion partners that can be used for expression of disulfide-rich aggregation-prone proteins. Alternatively, it might reveal that the effect of MBP is specific, which should be helpful in understanding the latter effect at the molecular level.

## ACKNOWLEDGMENT

We thank Véronique Chitarra, Shirley Longacre, Muriel Delepierre, and Graham Bentley for allowing us to use unpublished data of the protein expressed in insect cells and Graham Bentley for kindly providing the coordinates of the X-ray structure of the F19 fragment. The 600 MHz NMR spectrometer was funded by the Institut Pasteur and the Conseil Régional de l'Ile de France.

## REFERENCES

1. Kapust, R. B., and Waugh, D. S. (1999) *Protein Sci. 8*, 1668−74.
2. Giuliani, C. D., Iemma, M. R., Bondioli, A. C., Souza, D. H., Ferreira, L. L., Amaral, A. C., Salvini, T. F., and Selistre-de-Araujo, H. S. (2001) *Toxicon. 39*, 1595−600.
3. Nomine, Y., Ristriani, T., Laurent, C., Lefevre, J. F., Weiss, E., and Trave, G. (2001) *Protein Eng. 14*, 297−305.
4. Pryor, K. D., and Leiting, B. (1997) *Protein Expr. Purif. 10*, 309−19.
5. Hammarstrom, M., Hellgren, N., van Den Berg, S., Berglund, H., and Hard, T. (2002) *Protein Sci. 11*, 313−21.
6. Holder, A. A., Blackman, M. J., Burghaus, P. A., Chappel, J. A., Ling, I. T., McCallum-Deighton, N., and Shai, S. (1992) *Mem. Inst. Oswaldo Cruz 87 Suppl. 3*, 37−42.
7. Good, M. F., Kaslow, D. C., and Miller, L. H. (1998) *Annu. Rev. Immunol. 16*, 57−87.
8. Blackman, M. J., Heidrich, H. G., Donachie, S., McBride, J. S., and Holder, A. A. (1990) *J. Exp. Med. 172*, 379−82.
9. Chappel, J. A., and Holder, A. A. (1993) *Mol. Biochem. Parasitol. 60*, 303−11.
10. Morgan, W. D., Birdsall, B., Frenkiel, T. A., Gradwell, M. G., Burghaus, P. A., Syed, S. E. H., Uthaipibull, C., Holder, A. A., and Feeney, J. (1999) *J. Mol. Biol. 289*, 113−22.
11. Pizarro, J. C., Chitarra, V., Calvet, C., Verger, D., and Bentley, G. A. (2002) *Acta Crystallogr., Sect. D 58*, 1246−1248.
12. Betton, J. M., Sassoon, N., Hofnung, M., and Laurent, M. (1998) *J. Biol. Chem. 273*, 8897−902.
13. Chung, C. T., Niemela, S. L., and Miller, R. H. (1989) *Proc. Natl. Acad. Sci. U.S.A. 86*, 2172−5.
14. Miller, J. H. (1972) *Experiments in Molecular Genetics*, p 466, Cold Spring Harbor Laboratory, Woodbury, New York.
15. Wang, J., Betton, J. M., Michel, V., Hofnung, M., and Charbit, A. (1997) *Mol. Microbiol. 26*, 1141−3.
16. Chang, S. P., Kramer, K. J., Yamaga, K. M., Kato, A., Case, S. E., and Siddiqui, W. A. (1988) *Exp. Parasitol. 67*, 1−11.
17. Pace, C. N., Vajdos, F., Fee, L., Grimsley, G., and Gray, T. (1995) *Protein Sci. 4*, 2411−23.
18. Laemmli, U. K. (1970) *Nature 227*, 680−5.
19. Morrissey, J. H. (1981) *Anal. Biochem. 117*, 307−10.
20. Friguet, B., Chaffotte, A. F., Djavadi-Ohaniance, L., and Goldberg, M. E. (1985) *J. Immunol. Methods 77*, 305−19.
21. Manavalan, P., and Johnson, W. C. J. (1987) *Anal. Biochem. 167*, 76−85.
22. Johnson, B. A., and Blevins, R. A. (1994) *J. Biomol. NMR 4*, 603−14.
23. States, D. J., Haberkorn, R. A., and Ruben, D. J. (1982) *J. Magn. Reson. 48*, 286−92.
24. Griesinger, C., Otting, G., Wüthrich, K., and Ernst, R. R. (1988) *J. Am. Chem. Soc. 110*, 7870−2.
25. Bax, A., and Davis, D. G. (1985) *J. Magn. Reson. 65*, 355−60.
26. Piotto, M., Saudek, V., and Sklenár, V. (1992) *J. Biomol. NMR 2*, 661−5.
27. Liu, M. L., Mao, X.-A., Ye, C. H., Huang, H., Nicholson, J. K., and Lindon, J. C. (1998) *J. Magn. Reson. 132*, 125−9.
28. Jones, J. A., Wilkins, D. K., Smith, L. J., and Dobson, C. M. (1997) *J. Biomol. NMR 10*, 199−203.
29. Wilkins, D. K., Grimshaw, S. B., Receveur, V., Dobson, C. M., Jones, J. A., and Smith, L. J. (1999) *Biochemistry 38*, 16424−31.
30. Chang, J. Y., Li, L., and Lai, P. H. (2001) *J. Biol. Chem. 276*, 4845−52.
31. Chaffotte, A. F., Guillou, Y., Delepierre, M., Hinz, H.-J., and Goldberg, M. E. (1991) *Biochemistry 30*, 8067−73.
32. Guijarro, J. I., Jackson, M., Chaffotte, A. F., Delepierre, M., Mantsch, H. H., and Goldberg, M. E. (1995) *Biochemistry 34*, 2998−3008.
33. Bach, H., Mazor, Y., Shaky, S., Shoham-Lev, A., Berdichevsky, Y., Gutnick, D. L., and Benhar, I. (2001) *J. Mol. Biol. 312*, 79−93.
34. Hoischen, S. H., Vollmer, P., Marz, P., Ozbek, S., Gotze, K. S., Peschel, C., Jostock, T., Geib, T., Mullberg, J., Mechtersheimer, S., Fischer, M., Grotzinger, J., Galle, P. R., and Rose-John, S. (2000) *Eur. J. Biochem. 267*, 3604−12.
35. Huys, I., Dyason, K., Waelkens, E., Verdonck, F., van Zyl, J., du Plessis, J., Muller, G. J., van der Walt, J., Clynen, E., Schoofs, L., and Tytgat, J. (2002) *Eur. J. Biochem. 269*, 1854−65.
36. Anaguchi, H., Hiraoka, O., Yamasaki, K., Naito, S., and Ota, Y. (1995) *J. Biol. Chem. 270*, 27845−51.
37. Sachdev, D., and Chirgwin, J. M. (1998) *Protein Expr. Purif. 12*, 122−32.
38. Blondel, A., Nageotte, R., and Bedouelle, H. (1996) *Protein Eng. 9*, 231−8.
39. Brégégère, F., Schwartz, J., and Bedouelle, H. (1994) *Protein Eng. 7*, 271−80.
40. Koradi, R., Billeter, M., and Wüthrich, K. (1996) *J. Mol. Graphics 14*, 51−5.

BI035321C